Proceedings of the 1st Marine Energy Technology Symposium
METS2013
April 10-11, 2013, Washington, D.C.

TOWARD A SIMULATION-BASED APPROACH FOR OPTIMIZING MHK TURBINE ARRAYS IN NATURAL WATERWAYS

Xiaolei Yang
St. Anthony Falls Laboratory
Department of Civil Engineering
University of Minnesota
Minneapolis, MN 55414, USA

Seokkoo Kang
St. Anthony Falls Laboratory
Department of Civil Engineering
University of Minnesota
Minneapolis, MN 55414, USA

Fotis Sotiropoulos *
St. Anthony Falls Laboratory
Department of Civil Engineering
University of Minnesota
Minneapolis, MN 55414, USA

ABSTRACT

In this paper, we develop a powerful computational framework toward simulating marine and hydrokinetic (MHK) turbine arrays mounted in complex river bathymetry. The computational approach employs high resolution large-eddy simulation (LES) with the turbines parameterized as actuator disks. Arbitrarily complex river bathymetry is represented by the curvilinear immersed boundary (CURVIB) method. Water surface is modeled using level set method. We validate the present method by simulating flow over an axial-flow hydrokinetic turbine mounted on the bed of an open channel. Simulations of flow over a column of turbines with three different streamwise turbine spacings are then carried out.

INTRODUCTION

MHK energy from free-flowing waves, tides and currents comprises an important source of clean and renewable energy. Untapped MHK energy resources in the U.S. have the potential to provide up to ten percent of the Nation's electricity as noted in the U.S. Marine and Hydrokinetic Renewable Energy Roadmap in 2011. However, the development of technologies for harnessing MHK energy is still at early stage. The hydrodynamics of MHK turbines arrays and the impacts of MHK turbines arrays on aquatic and ecosystems remain today largely unexplored and poorly understood. Computational fluid dynamics (CFD) serves as a powerful tool for investigating hydrodynamics of MHK turbine arrays, which has been widely applied in simulating the flow over wind turbines [1–4]. However the applications to MHK turbines are limited.

Turbines need to be parameterized in order to avoid the computational cost to resolve the boundary layer around the turbine blades. In actuator disk parameterization, the turbine is represented as a permeable disk which extracts momentum from the flow. The forces distributed on the disk are calculated from one-dimensional momentum theory. Using the actuator disk parameterization, Sun et al. [5] studied the free surface changes and wake behaviors of flow past a tidal turbine using the commercial software Fluent. MacLeod et al. [6] simulated the flows past two tandem turbines. The actuator disk model cannot capture the rotation of turbines (an actuator disk model with rotation was developed in [7]) and is limited by the assumptions for the one-dimensional momentum theory. To overcome these shortcomings of the actuator disk model, an actuator line model is proposed in [1]. In the actuator line model the turbine blade is represented by an actuator line with distributed forces. Using actuator line model Churchfield et al. [8] simulated wake propagation and power production of an tidal-current turbine array. Instead of parameterizing the turbines as actuator disks or actuator lines, the geometry of turbines can also be directly resolved using immersed boundary method [9]. In [10] Kang et al. simulated the three-dimensional, turbulent flow past an axial-flow MHK turbine mounted on the bed of a rectangular open channel by directly resolving the complex turbine geometry. For simulating the turbulent flows, RANS (Reynolds averaged NavierStokes equations) method is employed in [5,11] and LES method is used in [8, 10]. Compared with RANS method, LES method can directly capture the unsteady energetic large-scale flows, which may influence the turbine performance significantly. Turbine wake recoveries depend on the turbulence of the incoming flow. Uniform incoming flow was employed in [5]. Gant and Stallard [11] compared the Von Karman spectral approach and Syn-

*Corresponding Author: fotis@umn.edu

thetic Eddy Method (SEM) for generating inflow turbulence for simulating flow past a tidal turbine. In [8, 10], the turbulent inflows were generated from a precursor fully developed channel flow simulation. Different from wind turbine applications, MHK turbines have interactions with the water-air interfaces. In [5] the water-air interface is captured using the volume of fluid (VOF) method.

In this work a computational frame work for simulating MHK turbine arrays in natural waterways is developed. The turbulent flow is simulated using LES method [12] with turbulence of the incoming flow generated from a fully developed turbulent channel flow. The complex bathymetries are represented by curvilinear immersed boundary (CURVIB) method [9]. The water-air interface is simulated using level set method [13]. The turbines are modeled using actuator disk model [4, 14] or actuator line model. As the first step of this work the actuator disk model is employed in this paper, validated by experimental measurements and applied to simulate turbine arrays with different spacings in an open channel.

NUMERICAL METHODS

Governing equation

The LES equations governing the incompressible turbulent flows are the 3D, unsteady, filtered continuity and Navier-Stokes equations. In this method the governing equations are first written in Cartesian coordinates x_i and then transformed fully (both the velocity vector and spatial coordinates are expressed in curvilinear coordinates) in non-orthogonal, generalized, curvilinear coordinates ξ^i. The transformed equations read in compact tensor notation (repeated indices imply summation) as follows $(i, j = 1, 2, 3)$:

$$J\frac{\partial U^j}{\partial \xi^j} = 0, \tag{1}$$

$$\begin{aligned}\frac{1}{J}\frac{\partial U^i}{\partial t} =& \frac{\xi_l^i}{J}\left(-\frac{\partial}{\partial \xi^j}(U^j u_l) + \frac{\mu}{\rho}\frac{\partial}{\partial \xi^j}\left(\frac{g^{jk}}{J}\frac{\partial u_l}{\partial \xi^k}\right)\right.\\ &\left.-\frac{1}{\rho}\frac{\partial}{\partial \xi^j}(\frac{\xi_l^j p}{J}) - \frac{1}{\rho}\frac{\partial \tau_{lj}}{\partial \xi^j} + f_i\right),\end{aligned} \tag{2}$$

where $\xi_l^i = \partial \xi^i / \partial x_l$ are the transformation metrics, J is the Jacobian of the geometric transformation, u_i is the i^{th} component of the velocity vector in Cartesian coordinates, U^i=$(\xi_m^i/J)u_m$ is the contravariant volume flux, $g^{jk} = \xi_l^j \xi_l^k$ are the components of the contravariant metric tensor, ρ is the density, μ is the dynamic viscosity, p is the pressure, $f_i (i = 1, 2, 3)$ are the body forces introduced by the turbines and τ_{ij} represents the anisotropic part of the subgrid scale stress tensor, which is modeled by the eddy-viscosity subgrid scale model. At the bottom boundary, the shear stress boundary condition and no-flux boundary condition are used for the wall-parallel and wall-normal velocity components, respectively. The wall shear stress is calculated from the logarithmic law for rough wall [4]. For a smooth wall, the wall shear stress is calculated from a simplified boundary layer equation [4]. Arbitrarily complex geometries are represented by the CURVIB method [9]. For details of the numerical schemes, please refer [12].

Actuator disk model

In the actuator disk model a turbine rotor is represented by a permeable circular disk that is discretized using an unstructured triangular grid. Drag forces exerted by the turbine rotor on flow are uniformly distributed over the disk surface to model the momentum extraction by a turbine rotor. The thrust force on the turbine rotor is calculated from the following expression

$$F_T = \frac{1}{2}\rho C_T U_\infty^2 \frac{\pi}{4} D^2, \tag{3}$$

where ρ is the air density, C_T is the thrust coefficient, U_∞ is the incoming velocity and D is the diameter of turbine rotor. In the present work, the thrust coefficient C_T is determined from the one-dimensional momentum theory and reads as

$$C_T = 4a(1-a), \tag{4}$$

where a is the axial induction factor of the turbine rotor, which can be specified, from actuator line simulation or from geometry-resolving simulation. Generally, the positions of grid nodes of the actuator disk do not coincide with those of the background (fluid) domain. Quantities are transferred between the two grids through discrete delta functions [15]. Please refer to [4] for the details about the implementation the actuator disk model.

Level set method

The motion of the free surface is modeled using level set method. The level set function ϕ on cuvilinear grids is determined by the equation shown as follows:

$$\frac{1}{J}\frac{\partial \phi}{\partial t} + U^j \frac{\partial \phi}{\partial \xi^j} = 0. \tag{5}$$

In order to keep the level set function satisfy $|\nabla \phi| = 1$ and guarantee the conservation of mass, a mass conserving reinitialization equation proposed by Sussman and Fatemi is solved [16]. For the details of the implementation of the level set method in the CURVIB method, please refer to [13]

RESULTS

We apply our method to simulate the flows past an axial-flow hydrokinetic turbine and several turbines mounted on the bed of an open channel. The computational domain is 25 m long (streamwise direction x), 2.75 m wide (crosswise direction y) and 1.8 m deep (vertical direction z), which has the same width and depth with the experiment carried at Saint Anthony Falls Laboratory (SAFL), University of Minnesota [17]. The rotor diameter of the model turbine is $D = 0.5m$. The hub height of the turbine is $h_{hub} = 0.425m$. In the simulated the (first) turbine is located at the middle of channel and 10 m from the inlet boundary. The number of grid cells is 1000, 110 and 110 in the x, y and z directions, respectively. No slip boundary conditions are employed at the two-side walls. At the bottom, wall model is applied with the roughness height of the bed is $0.0062m$. The inflow velocity field is generated from periodical turbulent open channel flows. The bulk velocity of the water is $U_b = 0.4ms^{-1}$. The flow depth is initially set as 1.15 m. For the air, free-slip and non-penetration boundary condition are applied to the parallel and normal velocity components, respectively. For the air part, the density is $1.204kgm^{-3}$ and the dynamic viscosity of the air is $1.8 \times 10^{-5}kgm^{-1}s^{-1}$. The density and dynamic viscosity of the water are $1000kgm^{-3}$ and 1×10^{-3}, respectively. The induction factor of the turbine is fixed at 0.36.

Validation: One turbine case

The comparisons of the present computed results for the one turbine case with the experimental results [17] are shown in this section. In Figure 1, we show the comparisons of the time-averaged streamwise velocity profiles at different downstream locations. At $1D$ downstream location as shown in Figure 1a, the present method predicts very well for the upper part above the hub part while underpredict and overpredict the velocity deficits in the middle and lower parts of the turbine. At $2D$ downstream location as shown in Figure 1b, the velocity deficit in the middle is still underpredicted while good agreements are obtained for the outer parts. At the $3D$, $5D$, $7D$ and $10D$ downstream locations as shown in Figures. 1c, 1d, 1e and 1f, respectively, good agreements of the velocity profiles with the experimental measurements are obtained.

Figure 2 shows the comparisons of the computed turbulence kinetic energy (TKE) with the measurements. At $1D$ (Figure 2a) and $2D$ (Figure 2b) downstream locations, the present model predicts very well the two peaks of TKE at the top tip and bottom tip of the turbine while fails to predict the peak of TKE around the hub height of turbine. This is probably because the effects of nacelle and the tower are not included in the present actuator disk model. Thus, the complex interactions of the shear layer generated at the edge of turbines with the one generated at the hub cannot be captured. At $3D$ downstream location as shown in Figure 2c, the two peaks of TKE are well captured while the overall TKE is underpredicted. Better agreements with measurements are obtained for further downstream locations (form 5D). However, the TKE is still somewhat underpredicted at these locations (5D, 7D and 10D in Figures 2d, 2e and 2f, respectively).

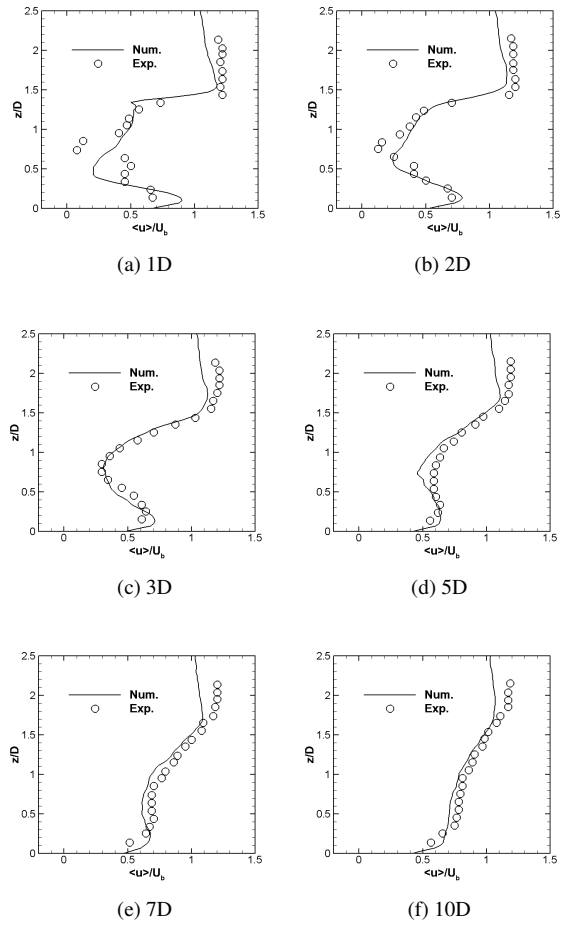

FIGURE 1: Comparisons of the time-averaged streamwise velocity at different downstream locations.

We compare the Reynolds shear stress $< uw >$ at different downstream locations with measurements in Figure 3. Similar to the comparisons for the mean streamwise velocity and TKE, the present model fails to predict the complex variations of $< uw >$ at near wake locations (1D and 2D as shown in Figures 3a and 3b, respectively). At further downstream locations, on the other hand, very good agreements with the measurements are obtained as shown in Figures 3c, 3d, 3e and 3f for $3D$, $5D$, $7D$ and $10D$ downstream locations, respectively.

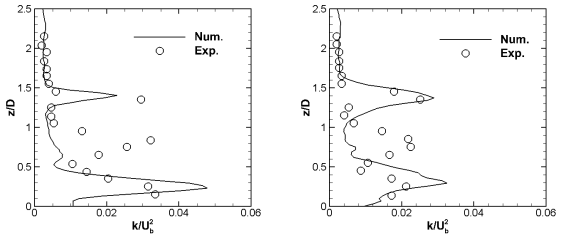

(a) 1D (b) 2D

(c) 3D (d) 5D

(e) 7D (f) 10D

FIGURE 2: Comparisons of the turbulence kinetic energy at different downstream locations.

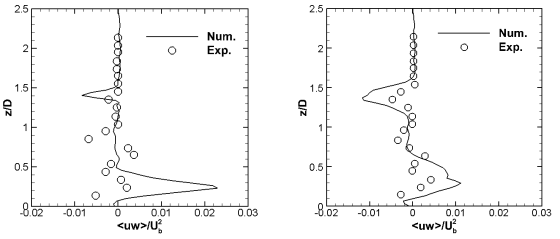

(a) 1D (b) 2D

(c) 3D (d) 5D

(e) 7D (f) 10D

FIGURE 3: Comparisons of the Reynolds shear stress $\langle uw \rangle$ at different downstream locations.

Flows past arrays of axial-flow hydrokinetic turbines

In this section, we apply the method to simulate a column of turbines placed in the same channel. Three different streamwise spacings are considered, which are 3D, 5D and 7D, respectively.

The contours of the time-averaged streamwise velocity on the x-z plane through the center of turbines are shown in Figure 4. The velocity is normalized using bulk velocity. From top to bottom, we show the 3D, 5D and 7D cases, respectively. For the case with 3D spacing, it is seen that the wake from the first turbine is still very significant when the flow meets the second turbine. The superimposition of the wake from first turbine with the second turbine makes a very strong wake from the second turbine. The strengths of the wakes from the third to the sixth turbines are very similar while the wake from the seventh turbine is somewhat weaker than those from upstream turbines. For the 3D spacing case as shown in the middle of Figure 4, the wake from the first turbine still interacts the wake from the second one, which make the strength of the wake from the second turbine is much stronger than the other wakes. For the case with 7D spacing, on the other hand, the wake from the first turbine has little interactions with the wake from the second turbine.

We show the contours of the computed turbulence kinetic energy on the x-z plane through the center of turbines in Figure 5. For the case with 3D spacing as shown on the top of Figure 5, the strengths of TKE in the upper shear layers are much larger than those in the bottom shear layers. The strength of TKE is weakest for the first turbine, increases for the second to the fourth turbines and is strongest for the fifth to the seventh turbines. For the sixth and seventh turbines, significant TKE even exist in the bottom shear layers. The case with 5D spacing is shown in the middle of Figure 5. As seen, the strengths of the TKE is much weaker than that from the case with 3D spacing. Largest TKE is obtained at fifth turbine. The strength of the TKE from the case with 7D spacing as shown at the bottom of Figure 5 is the weakest in these

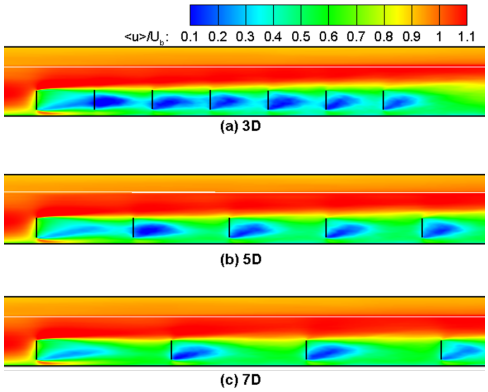

FIGURE 4: Contours of the time-averaged streamwise velocity on the x-z plane through the center of turbines. The water surface is indicated by the white line.

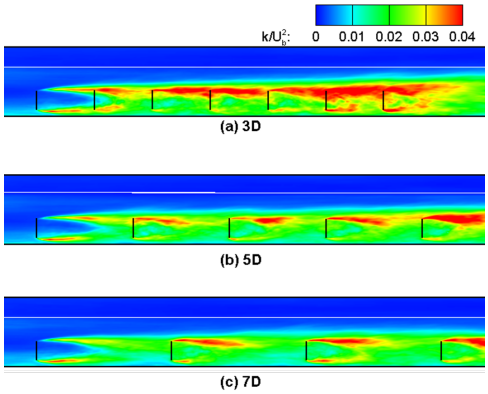

FIGURE 5: Contours of the turbulence kinetic energy on the x-z plane through the center of turbines.

three cases.

The extracted power of each turbine in the array are compared with that from the stand-alone turbine as shown in Figure 6. P denotes the power from the turbine in the array and P_0 denotes the power from the stand-alone turbine, which is from last section. The first turbines from all the three cases produce almost the same power with that from the single turbine. Quite different behaviors for the downstream turbines are obtained for the three cases. The power output from each turbine for the $3D$ spacing is lowest in these three cases, while it is highest for the case with $7D$ spacing. For the cases with $3D$ and $5D$, the second turbines produce the lowest power in all the simulated turbines. For the case with $7D$ spacing, the power output from the second turbine, on the other hand, is somewhat larger than those from further downstream turbines.

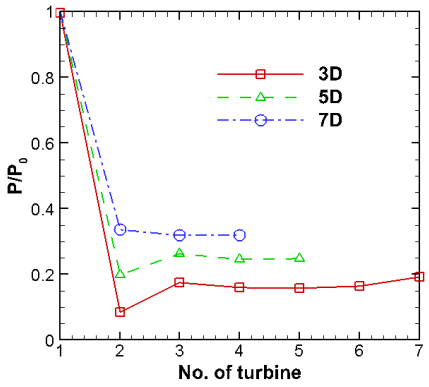

FIGURE 6: The ratios of the power extracted by the turbines in the arrays to the power extracted by a stand-alone turbine.

CONCLUSIONS

In the present method for simulating the flow over marine and hydrokinetic (MHK) turbine arrays mounted in complex river bathymetry, actuator disk model is used for the MHK turbine, free water surface is modeled using level set method and the complex bathymetry is represented using CURVIB method. In this paper, we validate the present method with actuator disk model for the turbine and level set method for the free surface by comparing the computed results with the measurements for the flow over an axil-flow hydrokinetic turbine. Discrepancies are observed in the near wake (1D and 2D downstream locations). Very good agreements are obtained for further downstream locations ($\geq 3D$).

Three cases for a column of turbines, with streamwise spacing $3D$, $5D$ and $7D$, respectively, are also investigated. It is observed that the power output for the second turbine decreased significantly for the cases with $3D$ and $5D$ spacing, in which the power from the second turbine are smaller than those from the further downstream turbines. For the $7D$ case, on the other hand, the power output from the second turbine are second turbine is somewhat higher than further downstream turbines. Significant TKE are observed for downstream turbines, especially for the $3D$ spacing case.

Studies on several columns of turbines and different layouts of turbines will be carried out in the future work. MHK turbines mounted on the bed of a natural meandering stream with complex bathymetry will also be investigated in the future.

ACKNOWLEDGMENT

This work was supported by Department of Energy DOE (DE-EE0002980) and Xcel Energy through the Renewable Development Fund (grant RD3-42). Computational resources were provided by the University of Minnesota Supercomputing Insti-

tute.

REFERENCES

[1] Sørensen, J. N., and Shen, W. Z., 2002. "Numerical modeling of wind turbine wakes". *J. Fluid Eng. Trans. ASME,* ***124***, pp. 393–399.

[2] Jimenez, A., Crespo, A., Migoya, E., and Garcia, J., 2007. "Advances in large-eddy simulation of a wind turbine wake". *Journal of Physics: Conference Series,* ***75***, p. 012041.

[3] Calaf, M., Meneveau, C., and Meyers, J., 2010. "Large eddy simulation study of fully developed wind-turbine array boundary layers". *Phys. Fluids,* ***22***, p. 015110.

[4] Yang, X., Kang, S., and Sotiropoulos, F., 2012. "Computational study and modeling of turbine spacing effects in infinite aligned wind farms". *Phys. Fluids,* ***24***, p. 115107.

[5] Sun, X., Chick, J., and Bryden, I., 2008. "Laboratory-scale simulation of energy extraction from tidal currents". *Renew. Energ.,* ***33***, pp. 1267–1274.

[6] MacLeod, A., Barnes, S., Rados, K., and Bryden, I. "Wake effects in tidal current turbine farms". *Proceedings of the MAREC Conference, Newcastle, September 2002*, pp. 49–53.

[7] Wu, Y.-T., and Porté-Agel, F., 2011. "Large-eddy simulation of wind-turbine wakes: Evaluation of turbine parametrisations". *Boundary-Layer Meteorol.,* ***138***, pp. 345–366.

[8] Churchfield, M., Li, Y., and Moriarty, P. "A large-eddy simulation study of wake propagation and power production in an array of tidal-current turbines". *9th European Wave and Tidal Energy Conference 2011 Southhampton, England September 4 9, 2011*, pp. NREL/CP–5000–51765.

[9] Ge, L., and Sotiropoulos, F., 2007. "A numerical method for solving the 3d unsteady incompressible navier-stokes equations in curvilinear domains with complex immersed boundaries". *J. Comput. Phys.,* ***225***(2), pp. 1782–1809.

[10] Kang, S., Borazjani, I., Colby, J. A., and Sotiropoulos, F., 2012. "Numerical simulation of 3d flow past a real-life marine hydrokinetic turbine". *Adv. Water Resour.,* ***39***, pp. 33–43.

[11] Gant, S., and Stallard, T., 2008. "Modelling a tidal turbine in unsteady flow". *Proc. Int. Society Offshore and Polar Engineers, Vancouver, Canada*.

[12] Kang, S., Lightbody, A., Hill, C., and Sotiropoulos, F., 2011. "High-resolution numerical simulation of turbulence in natural waterways". *Adv. Water Resour.,* ***34***, pp. 98–113.

[13] Kang, S., and Sotiropoulos, F., 2012. "Numerical modeling of 3d turbulent free surface flow in natural waterways". *Advances in Water Resources,* ***40***, pp. 23–36.

[14] Yang, X., and Sotiropoulos, F. "On the predictive capabilities of les-actuator disk model in simulating turbulence past wind turbines and farms". *The 2013 American Control Conference, June 17 - 19, Washington, DC.*

[15] Yang, X., Zhang, X., Li, Z., and He, G.-W., 2009. "A smoothing technique for discrete delta functions with application to immersed boundary method in moving boundary simulations". *J. Comput. Phys.,* ***228***, pp. 7821–7836.

[16] M, S., and E., F., 1999. "An efficient, interface-preserving level set redistancing algorithm and its application to interfacial incompressible fluid flow". *SIAM J. Sci. Comput.,* ***20***, p. 11651191.

[17] Chamorro, L., Hill, C., Morton, S., Ellis, C., Arndt, R., and Sotiropoulos, F., 2013. "On the interaction between a turbulent open channel flow and an axial-flow turbine". *Journal of Fluid Mechanics,* ***716***, pp. 658–670.